Medical Physics
The International Journal of Medical Physics Research and Practice

Application of the optically stimulated luminescence (OSL) technique for mouse dosimetry in micro-CT imaging

Jean-Marc Vrigneaud, Alan Courteau, Julien Ranouil, Loïc Morgand, Olivier Raguin, Paul Walker, Alexandra Oudot, Bertrand Collin, and François Brunotte

Citation: Medical Physics **40**, 122102 (2013); doi: 10.1118/1.4829499
View online: http://dx.doi.org/10.1118/1.4829499
View Table of Contents: http://scitation.aip.org/content/aapm/journal/medphys/40/12?ver=pdfcov
Published by the American Association of Physicists in Medicine

Application of the optically stimulated luminescence (OSL) technique for mouse dosimetry in micro-CT imaging

Jean-Marc Vrigneaud[a] and Alan Courteau
Department of Nuclear Medicine, Centre Georges-François Leclerc, 1 rue Professeur Marion, Dijon 21079 Cedex, France

Julien Ranouil
Landauer Europe, 33 avenue du Général Leclerc, Fontenay-aux-Roses 92266 Cedex, France

Loïc Morgand and Olivier Raguin
Oncodesign, 20 rue Jean Mazen, Dijon 21076 Cedex, France

Paul Walker
LE2i CNRS UMR 5158, Faculty of Medicine, BP 87900, 21079 Dijon Cedex, France

Alexandra Oudot and Bertrand Collin
Department of Nuclear Medicine, Centre Georges-François Leclerc, 1 rue Professeur Marion, Dijon 21079 Cedex, France

François Brunotte
Department of Nuclear Medicine, Centre Georges-François Leclerc, 1 rue Professeur Marion, Dijon 21079 Cedex, France and LE2i CNRS UMR 5158, Faculty of Medicine, BP 87900, 21079 Dijon Cedex, France

(Received 17 May 2013; revised 1 September 2013; accepted for publication 15 October 2013; published 15 November 2013)

Purpose: Micro-CT is considered to be a powerful tool to investigate various models of disease on anesthetized animals. In longitudinal studies, the radiation dose delivered by the micro-CT to the same animal is a major concern as it could potentially induce spurious effects in experimental results. Optically stimulated luminescence dosimeters (OSLDs) are a relatively new kind of detector used in radiation dosimetry for medical applications. The aim of this work was to assess the dose delivered by the CT component of a micro-SPECT (single-photon emission computed tomography)/CT camera during a typical whole-body mouse study, using commercially available OSLDs based on Al_2O_3:C crystals.

Methods: CTDI (computed tomography dose index) was measured in micro-CT with a properly calibrated pencil ionization chamber using a rat-like phantom (60 mm in diameter) and a mouse-like phantom (30 mm in diameter). OSLDs were checked for reproducibility and linearity in the range of doses delivered by the micro-CT. Dose measurements obtained with OSLDs were compared to those of the ionization chamber to correct for the radiation quality dependence of OSLDs in the low-kV range. Doses to tissue were then investigated in phantoms and cadavers. A 30 mm diameter phantom, specifically designed to insert OSLDs, was used to assess radiation dose over a typical whole-body mouse imaging study. Eighteen healthy female BALB/c mice weighing 27.1 ± 0.8 g (1 SD) were euthanized for small animal measurements. OLSDs were placed externally or implanted internally in nine different locations by an experienced animal technician. Five commonly used micro-CT protocols were investigated.

Results: CTDI measurements were between 78.0 ± 2.1 and 110.7 ± 3.0 mGy for the rat-like phantom and between 169.3 ± 4.6 and 203.6 ± 5.5 mGy for the mouse-like phantom. On average, the displayed CTDI at the operator console was underestimated by 1.19 for the rat-like phantom and 2.36 for the mouse-like phantom. OSLDs exhibited a reproducibility of 2.4% and good linearity was found between 60 and 450 mGy. The energy scaling factor was calculated to be between 1.80 ± 0.16 and 1.86 ± 0.16, depending on protocol used. In phantoms, mean doses to tissue over a whole-body CT examination were ranging from 186.4 ± 7.6 to 234.9 ± 7.1 mGy. In mice, mean doses to tissue in the mouse trunk (thorax, abdomen, pelvis, and flanks) were between 213.0 ± 17.0 and 251.2 ± 13.4 mGy. Skin doses (3 OSLDs) were much higher with average doses between 350.6 ± 25.3 and 432.5 ± 34.1 mGy. The dose delivered during a topogram was found to be below 10 mGy. Use of the multimouse bed of the system gave a significantly 20%–40% lower dose per animal ($p < 0.05$).

Conclusions: Absorbed doses in micro-CT were found to be relatively high. In micro-SPECT/CT imaging, the micro-CT unit is mainly used to produce a localization frame. As a result, users should

pay attention to adjustable CT parameters so as to minimize the radiation dose and avoid any adverse radiation effects which may interfere with biological parameters studied. © *2013 American Association of Physicists in Medicine*. [http://dx.doi.org/10.1118/1.4829499]

Key words: OSL, mouse dosimetry, micro-CT

1. INTRODUCTION

For the past two decades, micro-CT has proven to be valuable in many different fields with applications well beyond the simple characterization of skeletal structures.[1,2] In preclinical research, micro-CT is a well-established technique to noninvasively investigate small animal models of disease. New drug therapies can be easily validated *in vivo* and in a cost-effective way, thanks to the relatively quick production of high-resolution images. However, the radiation dose delivered to small animals during a micro-CT scan has been known to be much higher than in clinical CT.[1] Indeed, theoretical formulas predict that, for a given noise level, the dose is inversely proportional to the fourth power of the cubic voxel size.[3] Considering the high sampling of current flat panel detectors used in micro-CT imaging and the processing capabilities of modern computing, the layman user may be easily tempted to increase the dose to unrealistic levels in order to obtain a good image quality.

Currently, micro-CT is also frequently associated with micro-PET (positron emission tomography) and/or micro-SPECT (single-photon emission computed tomography) in multimodality imaging platforms.[4] The anatomical information provided by CT is then used to precisely locate radiopharmaceutical uptakes highlighted by radionuclide imaging. Micro-CT can also be used for attenuation correction in order to perform absolute quantitative measurements on isotopic images. In these hybrid imaging techniques, the administered activity per unit body mass can be relatively high compared with those used clinically and the dose delivered by the micro-CT becomes even more a concern as it is added to the dose delivered by the administration of radiopharmaceuticals.

Several studies have been reporting radiation dose levels delivered by micro-CT, using either Monte Carlo calculations[5–7] or experimental measurements[8–12] (for a complete review of former studies, see Carlson[8]). Depending on the micro-CT protocols used, typical radiation absorbed dose in the range 17–760 mGy per scan were found. These dose levels have led some groups to raise concerns when it comes to serial micro-CT imaging used in longitudinal studies of the same animal.[10,13] On the other hand, recent studies investigating biological radiation damage or tumor growth in mouse models show no observable impact attributable to a potential radiation therapy effect due to low-voltage x-ray imaging.[14,15] As a result, it remains unclear whether the high level doses involved in micro-CT hamper the results of radiobiological studies. Until resolution of the effect, it is reasonable to optimize the CT-acquisitions parameters to keep the radiation dose as low as reasonably achievable (ALARA) with respect to image quality.

Up till now, dose measurements in preclinical imaging were mostly carried out with thermoluminescent dosimeters (TLDs) and ionization chambers. Optically stimulated luminescence dosimeters (OSLDs) are well-known detectors used in radiation protection and more recently in radiation therapy and diagnostic radiology for dosimetric applications.[16–18] Basically, the luminescence process of OSLDs is the same as in TLDs but OSLDs have numerous advantages. First, OSLD's radiation-induced luminescence is provoked by means of an external light stimulation instead of heat. As a result, the process of readout of OSLD is relatively easier, quicker, and the reader parameters are less complex to maintain. Also, the readout process can occur as early as 10 min after the end of irradiation and can be performed multiple times with little loss of signal.[16,18] In the radiation therapy energy range, OSLD exhibits almost no influence of energy, field size, angle, dose rate, and the signal appears to be stable for days.[19–21] Main drawbacks come from the complex change of OSLD sensitivity with high accumulated doses.[22] Also, energy and angular dependence have to be monitored with caution.[18,23] Finally, the main advantages of OSLDs are their robustness, ease of handling, and their relatively low cost-effectiveness. The recent availability of a commercial portable reader makes it possible to the endpoint user to control in-house the whole process of dosimetric characterization using a set of OSLD dosimeters. However, OSLDs are calibrated at a given radiation quality which do not necessarily correspond to the radiation quality needed by the user.

This work aims to investigate the radiation dose delivered by the CT component of the nanoSPECT/CT plus™ camera (Bioscan Inc., Washington, DC, USA) during a typical whole-body mouse imaging. To measure radiation doses in both study of phantoms and cadavers, a batch of OSLDs was used in association with the InLight™ MicroStar™ reader (Landauer Europe, Fontenay-aux-roses, France). The reader is designed exclusively for use with Al_2O_3:C Inlight™ dosimeters. The energy response of the OSL detectors was corrected for suitable use in the low-kV range by defining a specific energy correction factor to be applied to OSLDs calibrated by the manufacturer. Micro-CT protocols used in our laboratory were investigated to assess the impact of the dose delivered in longitudinal studies of the same animals. Results obtained with OSLDs were compared with similar data available in the literature from measurements performed with TLDs and ionization chambers.

2. MATERIALS AND METHODS

2.A. Micro-CT system, scan protocols

The CT scanner used in this study was the micro-CT component of the nanoSPECT/CT plus™ preclinical camera

TABLE I. Acquisition parameters, displayed CTDI for the 19 micro-CT protocols used in this study. Protocols L1–L5 were investigated at each voltage setting.

	CT parameters							
Protocol identification	Type of acquisition	Tube potential (kVp)	Tube current (μA)	Exposure time (ms)	Number of projections	Pitch	mAs per rotation	Displayed CTDI (mGy)
M0	Topogram	55	145	1000	...	...	...	...
M1	Helical	45	177	1000	240	1	42	74
M2	Helical	55	145	1000	240	1	35	82
M3	Helical	65	123	1000	240	1	30	82
L1	Axial	45/55/65	177/145/123	500	180	...	16/13/11	28/31/31
L2	Axial	45/55/65	177/145/123	1000	180	...	32/26/22	55/61/61
L3	Axial	45/55/65	177/145/123	1000	240	...	42/35/30	74/82/82
L4	Axial	45/55/65	177/145/123	1000	360	...	64/52/44	111/122/123
L5	Axial	45/55/65	177/145/123	1500	360	...	96/78/66	166/184/184

(Bioscan Inc., Washington, DC, USA). On this system, the x-ray source and detector array are embedded in the gantry behind the gamma-camera detectors. The scanner acquires helical CT scans by rotating around a horizontal rotation axis, along which the small animals are positioned in the various imaging cell supports available with the Minerve systems (Minerve, Esternay, France). The x-ray source consisted of a miniature x-ray tube combined with a high voltage power supply in a single package (Thermo Fisher scientific Inc., Waltham, USA). The 90 kVp source featured a measured focal spot size of 12 μm from which the x rays emerge through a 127 μm thick beryllium window in a cone with approximate angle of 40°. The micro-CT detector consisted of an indirect-detection CMOS flat-panel with a 1024 × 2048 pixel photodiode array (Rad-Icon imaging Corp., Sunnyvale, USA). Considering the 48-μm pixel size and the fixed geometric magnification of the CT assembly (1.3), the nominal axial field of view (FOV) was 37.8 mm at isocenter.

In user mode, which was the exclusive mode used in this study, the choice of voltage settings was limited to 45, 55, and 65 kVp and the tube current was automatically adjusted to keep the beam power under the limit of the system. The tube current values were 177, 145, and 123 μA at, respectively, 45, 55, and 65 kV. Since the tube current was a fixed value at any selected voltage, the exposure was user-adjustable with the number of projections over a 360° CT acquisition and the time per projection. Each CT scan could be preceded by a localization scan, also referred to as either a scout scan or topogram, to define the axial examination range. When used, the topogram was always acquired with the same voltage (55 kVp) and the same exposure time (1000 ms). Table I summarizes the details of the CT-imaging parameters that were investigated in this study. Protocol M0 refers to the topogram described above. Protocols M1, M2, and M3 were representative of the "average" imaging parameters commonly used in our laboratory with a nominal tube voltage of, respectively, 45, 55, and 65 kVp. Protocols L1–L5 were chosen to check the linearity response of OSLD in the entire dose range delivered by the micro-CT for a total of 15 data points. Typical acquisition times for a whole-body mouse imaging study ranged from 3 to 30 min. For each acquisition, the manufacturer's calculated computed tomography dose index (CTDI) was displayed and recorded at the operator's console.

2.B. CT dose index in micro-CT imaging

At this time, no general consensus exists to recommend specifications for dosimetry phantoms in micro-CT imaging. So far, a range of diameters of 20–30 mm (mouse type) and 30–60 mm (rat type) have typically been used in small animal studies to represent realistic sizes of rodents.[24,25] According to the manufacturer, the CTDI displayed at the operator console of the camera is calculated using a rat-like phantom which is a 60 mm diameter cylinder made of polymethyl methacrylate (PMMA). However, a smaller phantom would be more appropriate to assess radiation dose for mice. In this study, a 30 mm diameter cylinder PMMA phantom, hereafter referred as phantom A, was chosen to mimic mouse dimensions (Fig. 1). CTDI was also measured in a 60 mm diameter phantom to verify the value calculated by the manufacturer. To this end, a 100 mm clinical CT ionization chamber (Type 30009 from PTW, Freiburg, Germany) connected to a dedicated electrometer (Unidos^{TM} T10001, PTW, Freiburg, Germany) was used. CTDI was determined by the following expression:

$$\mathrm{CTDI} = R \times K_{\mathrm{T,P}} \times N_{\mathrm{K}} \times \mathrm{Col}^{-1}, \quad (1)$$

FIG. 1. Phantom A (right) for CTDI measurements with a pencil ionization chamber and phantom B (left) for dose measurements with OSLDs. Both phantoms had a diameter of 30 mm.

TABLE II. Beam qualities used for the calibration of the CT-ionization chamber in the preclinical energy range (PTW, Freiburg, Germany). RQT 9 corresponds to the calibration settings usually encountered in clinical imaging.

Beam quality	Nominal tube voltage (kVp)	Filtration (mm)	Half-value layer (mm Al)
RQR2	40	2.5 Al	1.44
RQR3	50	2.5 Al	1.86
RQR4	60	2.5 Al	2.20
RQT9	120	3.5 Al + 0.25 Cu	8.38

where R is the pencil ionization chamber reading (C), $K_{T,P}$ is the correction factor for temperature and pressure, N_K is the calibration factor for the chamber expressed in air kerma for normal temperature and pressure (Gy × cm/C), and Col is the total nominal beam width (cm). As with clinical CT, the pencil ionization chamber was inserted in the central bore of each PMMA cylinder and positioned at the axis of rotation. Unlike clinical CT, no measurements were performed in the periphery of phantoms because of the small dimensions of rodent phantoms.[26] CTDI measurements were repeated three times according to parameters of protocols M1, M2, and M3 used in axial mode, with only one rotation of the tube (Table I).

Special care was given to the air kerma calibration of this chamber in the energy range of the x-ray beam delivered by the micro-CT as conventional CT ionization chamber is usually calibrated in reference to RQT9 IEC beam quality.[27]

Because the RQT9 beam quality is substantially higher than the typical spectrum used in micro-CT applications, specific calibrations at more similar x-ray spectra were requested from the CT-chamber's manufacturer (Table II). Because no intermediate calibration was possible to account for differences between the IEC beam qualities RQR2, RQR3, and RQR4 and our specific x-ray spectra, a comparison of half-value layer (HVL) was completed. HVL was measured in the topogram mode using a diagnostic kV sensor (type 40 X12-W from Radcal, Monrovia, USA) connected to an associated Accupro™ electrometer. Performance characteristics of the sensor for HVL determination were quoted as 10% of the value plus 0.3 mm Al.

2.C. OSL dosimeters

Dosimeters used in this study were OSLDs provided by Landauer Europe (Fontenay-aux-roses, France). The so-called nanoDot dosimeters are 0.4 cm diameter, 0.02 cm thick disks of Al_2O_3:C (aluminium oxide doped with carbon) encapsulated in a light-tight plastic holder with dimensions of 1.0 × 1.0 × 0.2 cm^3. The plastic cover is 0.037 g/cm^2 thick which, theoretically, makes the nanoDot an attractive surface-dose detector. Dosimeters were readout by the associated portable Inlight™ MicroStar™ reader (Landauer Europe, Fontenay-aux-roses, France). The readout process uses a light emitting diode (LED) array to stimulate the OSLD which, in turn, re-emit light, detected and measured by a photomultiplier tube (PMT). The reader was operated in continuous wave mode in which the optical stimulation light and the PMT are continually on and narrow-band optical filters are used to discriminate between the stimulation and emission light. The LED-filter combination has a peak emission at 532 nm and the PMT is filtered by a glass bandpass filter providing a peak sensitivity at 420 nm. In the default operating mode, the reader uses two calibration curves to convert PMT counts to dose and automatically switches between these two curves by comparing some test counts produced by a brief flash of light with a crossover value set by the manufacturer. The two calibration curves refer to the "low-dose" mode and the "high-dose" mode. The "low-dose" mode actually corresponds to a high optical stimulation whereas the "high-dose" mode refers to a reduced optical stimulation to prevent saturation of the PMT and to extend the dynamic range of the reader. For all measurements in this study, the illumination-read period was set to 2 s, which led to PMT counts ranging from 27 000 to 158 000 over the range of doses investigated in the "high-dose" mode (Sec. 3.D).

According to the manufacturer, the nanoDot OSLD are suitable for photons detection between 5 keV and 40 MeV with a lower limit of detection of 0.05 mGy. They can be ordered from two different categories: screened and unscreened. Screened dosimeters are selected OSLDs from a batch of preirradiated dosimeters with a NIST-traceable calibrated Cs-137 gamma source. Their individual sensitivity is selected to be within 1% (1 SD) of the value measured with reference nanoDots whose sensitivity is known to a high degree of accuracy and precision. Unscreened dosimeters are not preselected and are specified by the manufacturer to have an individual detector sensitivity of ±3% (1 SD) the sensitivity measured with reference nanoDots. A total of 207 unscreened dosimeters were used in this study. From this batch, 45 OSLDs were randomly extracted for checking reproducibility and linearity in the low-energy range of the micro-CT used. For each measurement in this study, OSLDs were first readout with the Inlight™ MicroStar™ reader to perform background subtraction. Then, they were exposed to photon radiation in different configurations described below. Finally, to avoid transient signal perturbation that occurs just after irradiation,[16,21] OSLDs were readout after a 30–60 min period. To maintain a large number of dosimeters for the small animal study, phantom experiments were repeated after optical bleaching of the OLSDs with the Pocket Annealer™ (Landauer Europe, Fontenay-aux-roses, France). The optical bleaching was performed by exposing OLSDs to a 5 cd sr (candela × steradian) LED lamp for 120 s. This duration was found to be acceptable to achieve a residual OSL signal of no more than four times the background level over the doses investigated with protocols M1, M2, and M3.

2.D. OLSD reproducibility and linearity

Thirty unscreened OSLDs were used to check the reproducibility of the dosimeters in the small-animal geometry of

irradiation of the nanoSPECT/CT plus™ camera. A PMMA phantom which fit into the mouse bed of the system was specifically designed to insert OSLDs aligned in single file (Fig. 1). The phantom consisted of two 280 mm-long solid semicylinders with one of the semicylinders having a central groove of width 11 mm and depth 2.5 mm, over the entire length, so as to introduce the nanoDots. Once positioned one over the other, the complete cylinder, hereafter referred as phantom B, had a diameter of 30 mm to mimic the anatomical dimensions of a mouse. The phantom could hold 28 dosimeters. When partially filled, the air gap was left unfilled. Unlike clinical CT, the scatter to primary ratio has been found to be rather low in micro-CT imaging (<0.5), especially with small phantom sizes.[28] For each protocol M1, M2, and M3, ten OSLDs were inserted in the central groove, one after the other, placed on the same side, in the same orientation and carefully secured with a tape. Long-axis centering of the dosimeters was performed with reference to radiopaque markers that were previously positioned in the central groove during a topogram acquisition with the phantom placed in a reproducible position on the mouse bed. The markers delimited a 60 mm scan range that was recorded for all subsequent CT acquisitions. The scan range of the system is defined as the reconstruction range, i.e., the distance between the first and last reconstructed slices. The actual scan range is increased by 0.5 FOV on each side to ensure sufficient projection data at both ends (a process known as over-scanning in helical CT). Therefore, the six central OSLDs were irradiated during the 360° full rotation of the micro-CT whereas the two other OSLDs on each side were partially irradiated during helical rotation. Dose measurements were repeated ten times for each voltage settings. Between each measurement, the nanoDots were optically bleached and then readout to perform background subtraction. Then, they were replaced in the phantom at exactly the same longitudinal position. Reproducibility of OSLDs response was reported as the coefficient of variation (CoV) obtained after these ten repeated acquisition with CT parameters corresponding to protocols M1, M2, and M3. X-ray output stability was assessed with the pencil ionization chamber used in the same irradiation configurations.

OSLD linearity was investigated in the range of doses available to the user using CT adjustable parameters. For this purpose, protocols L1–L5 were chosen so that the displayed CTDI scans the entire range of possible radiation dose delivered by the CT component of the Bioscan camera (Table I). Protocols L1–L5 were furthermore repeated at each voltage setting so as to cover the three voltages available to nanoSPECT/CT users. For each protocol, one OSLD was placed in the phantom B (Fig. 1) and irradiated during one rotation of the micro-CT, resulting in a total of 15 unscreened OSLDs used for this study. During each experiment, the OSLD was axially centered so as to be exactly in the middle of the CT length. Three measurements were repeated in the same configuration with the OSLD being optically bleached and readout before any new irradiation. Then, the low-energy calibrated CT-ionization chamber was inserted in the phantom A to measure the air kerma in the same configuration and with the same micro-CT protocols. The integrated absorbed dose was measured three times and compared to the data obtained with the OSLDs. Doses from the ionization chamber were corrected for each beam quality as stated in Sec. 2.B. Linear regression analysis was performed using GraphPad Prism version 6.02 for Windows (GraphPad Software, La Jolla, CA, USA, www.graphpad.com).

2.E. Energy correction of OLSDs

OSLD exhibits a dose response that depends highly on radiation quality in the diagnostic range.[18,21] The manufacturer provides sets of nanoDots that are exposed to a RQR6 RX beam quality to calibrate the Inlight™ MicroStar™ reader in the general field of diagnostic radiology.[29] The sets are composed of preirradiated OSLDs to known amounts of absorbed dose to air ranging from 0 to 1 Gy. The RQR6 beam quality corresponds to a nominal voltage of 80 kVp and a HVL of 2.9 mm Al. This calibration is said to yield results within ±6% for x-ray beam with mean energy between 34 and 54 keV. However, the mean energy quoted by the manufacturer must not be confused with the effective energy which can be calculated here to be around 33 keV using the HVL method.[30] In any case, the three user-adjustable voltage (45, 55, 65 kVp) of the nanoSPECT/CT camera needed an extra-correction to account for the rather lower spectral distribution of the x-ray beams.

In this study, the Inlight™ MicroStar™ Reader was used exclusively in the standard operating mode. In this mode, the system outputs the PMT counts divided by the given sensitivity of the OSLD and the air kerma calibration factor determined with the preirradiated OSLDs provided by the manufacturer at the RQR6 RX beam quality. To determine an extra energy correction factor to be applied in small animal imaging at each voltage, results from the linearity experiment were used. The slope of the line obtained at each kVp after linear regression analysis was assigned to be the energy correction factor between chamber ionization measurements (radiation quality corrected) and OSLD readings. Finally, the measured air kerma was converted to dose in tissue using the published ratio of mass energy absorption coefficients for tissue to air in the relevant energy range.[31] Therefore, the dose in tissue, D_{tissue}, was defined as

$$D_{\text{tissue}} = K_{\text{air,RQR6}} \times k_{\text{Q,RQR6}} \times \left(\frac{\mu_{\text{en}}}{\rho}\right)_{\text{air}}^{\text{tissue}}, \qquad (2)$$

where $K_{\text{air,RQR6}}$ is the air kerma measured with the reader calibrated for the RQR6 RX beam quality (mGy), $k_{\text{Q,RQR6}}$ is the specific energy correction factor that corrects for the effects of the difference between the RQR6 beam quality and the actual quality Q of the x-ray beams and $(\mu_{\text{en}}/\rho)_{\text{air}}^{\text{tissue}}$ is the ratio for tissue to air of the mass energy absorption coefficients. For this last term, the HVL method was used to assess the micro-CT effective energy at 45, 55, and 65 kVp.

2.F. Dose measurements in phantom and cadavers

From the 45 OSLDs used for reproducibility and linearity, 42 were optically bleached and reused for dose measurements

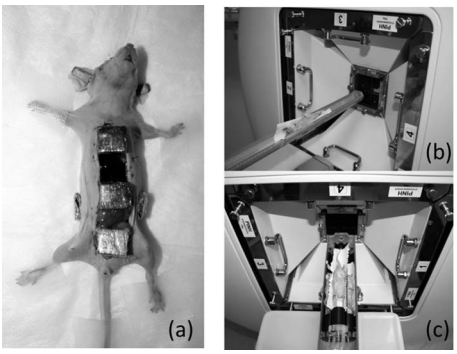

FIG. 2. (a) Schematic representation of the internal location of nanoDots within the mouse: in the thorax, in the liver, in the pelvis, and in the left and right flanks. For protocols M1, M2, and M3, mice were acquired in the prone position with the regular bed (b) and for protocols M2b, the multimouse bed of the camera was used (c).

in phantom B (Fig. 1). Protocols M1, M2, and M3 were investigated by acquiring a 10 cm long helical CT scan which mimics the common axial length of a whole-body mouse acquisition. For that purpose, 14 OSLDs (1 OSLD every cm) were inserted in the central groove of phantom B and CT acquisitions were performed such that ten OSLDs were located in the scan range while the four remaining OSLDs (two on each side) were partially irradiated during x-ray tube rotation. Spiral CT was acquired over exactly 10 cm with three helical rotations performed in 12 min. Three repeated acquisitions were carried out at each voltage with nanoDots being optically bleached and readout at each time. Dose in tissue was reported at each longitudinal position in phantom B.

Eighteen healthy female BALB/c mice weighing 27.1 ± 0.8 g (1 SD) were used for dose measurements. Animals were euthanized just prior to the experiments following regulations governing such work.[32] The OSLDs were first carefully wrapped in at least two layers of plastic wrap to prevent contamination from biological liquid substances and to protect the nanoDots. Then, for each mouse, nanoDots were placed externally or implanted internally in nine different locations by an experienced animal technician. The internal locations were: inside the brain, in the thoracic region, in the abdomen at the liver level, in the pelvis at the bladder level, and subcutaneous in the left and right flanks. These locations were chosen to match the main critical organs inside the mouse body, with respect to the relatively large size of the nanoDots. Also, the locations in the flanks were representative of implanted xenograft tumors, commonly studied in our laboratory. The external locations were: on the head, on the back, and between the hind legs of the mouse which was lying prone on the acquisition bed (Fig. 2). Nanodots were only used once resulting in a total of 162 OSLDs processed for the 18 mice.

Five different micro-CT protocols were used to perform the dose measurements on mice. All animals were first acquired with a topogram to set the range of the subsequent micro-CT acquisition. Accordingly, protocol M0 aimed at determining the absorbed dose delivered solely during a topogram with typical parameters used in our laboratory (see Sec. 2.A). During this topogram, the x-ray tube was oriented at 90° so as to obtain a side view of the mouse. The three "average" protocols M1, M2, and M3 were investigated (Table I). Protocol M2b differed from protocol M2 in that three mice were being simultaneously acquired on the multimouse bed of the system (Minerve, Esternay, France). For each protocol (M0, M1, M2, M2b, and M3), three different mice were acquired with the same examination length except for protocol M2b which was run twice with a total of six cadavers.

2.G. Statistical analysis

For CTDI measurements, uncertainties arose from the use of the pencil ionization chamber, the x-ray output stability of the micro-CT, and the reproducibility of dose measurements. For measurements with nanoDots, uncertainties were attributed to individual OSLDs sensitivity, x-ray output stability of the micro-CT, energy calibration procedure, and reproducibility of OSLD response. All these individual uncertainties were assessed, added in quadrature according to standard formulas and included in the data analysis.

Measurements with the pencil ionization chamber were subject to uncertainties on all the terms of Eq. (1). Uncertainty of the calibration coefficient of the ionization chamber was stated 2.5% (1 SD) on the calibration certificate. Considering the reading accuracy of our measuring instruments, standard uncertainty of the air density correction $K_{T,P}$ was assessed to be at most 0.5% [for a complete description, see IAEA-TECDOC-1585 (Ref. 33)]. A 0.8% (1 SD) uncertainty was assigned to the nominal beam width through measurements performed in the topogram mode with XR CT2 Gafchromic films (ISP technologies Inc.). X-ray output stability was given to be ±3% from 15 min to 24 h and from 45 to 90 kVp (Thermo Fisher scientific Inc., Waltham, USA). Considering the limited use of the micro-CT in the 45–65 kVp range and the small beam variations observed with the ionization chamber (see Sec. 3.B), it was chosen to neglect this uncertainty. Consequently, the combined standard uncertainty was $[(2.5\%)^2 + (0.5\%)^2 + (0.8\%)^2]^{1/2} = 2.7\%$ uncertainty for CTDI assessment with the ionization chamber.

Measurements with OSLDs were subject to uncertainties on all the terms of Eq. (2). Landauer's unscreened detectors were given as having an individual response variability of 3% (1 SD). It was chosen to keep this value which was believed to represent a conservative value. A 3% (1 SD) uncertainty was also assigned to the calibration calculation factor (counts/mGy) computed by the algorithm of the reader. Statistics of detected PMT counts were sufficient to neglect the contribution to overall uncertainty. The energy correction factors were derived from the slope of the linearity tests, in which both ionization chamber measurements and nanoDots measurements were subject to uncertainties. The graphical method of "limiting slopes"[34] was performed to obtain the uncertainties to be applied to the energy correction factors. For instance, given the 3% individual OSLDs sensitivity, the 3% uncertainty on the calibration factor and a 8.8% (1 SD) uncertainty calculated for the energy correction factor at 55 kVp,

TABLE III. Comparison of displayed and measured CTDI obtained with protocols M1, M2, and M3. Measured CTDIs were obtained in the 30 or 60 mm diameter PMMA phantom whereas displayed CTDI at the operator console was calculated solely for a 60 mm diameter PMMA phantom.

CTDI	Phantom's diameter (mm)	Protocol M1 (45 kVp)	Protocol M2 (55 kVp)	Protocol M3 (65 kVp)
Displayed (mGy)	60	74.0	82.0	82.0
Measured (mGy)	60	78.0 ± 2.1	96.7 ± 2.6	110.7 ± 3.0
Measured (mGy)	30	169.3 ± 4.6	189.8 ± 5.1	203.6 ± 5.5
Measured/displayed	60	1.05	1.18	1.35
Measured/displayed	30	2.29	2.31	2.48

the combined standard uncertainty was $[(3.0\%)^2 + (3.0\%)^2 + (8.8\%)^2]^{1/2} = 9.7\%$ uncertainty for measurements with nanoDots at 55 kVp.

Finally, the reproducibility of any experiment was quantified as a standard uncertainty which was added in quadrature to individual uncertainties described above.

3. RESULTS

3.A. HVL and CTDI measurements

Direct HVL measurements with a kV sensor were 1.63 ± 0.46 mm Al at 55 kVp and 1.89 ± 0.49 mm Al at 65 kVp. These measured HVLs were close to the IEC HVL values of 1.86 mm Al at 50 kVp and 2.20 mm Al at 60 kVp, used for calibration of the pencil ionization chamber (Table II). The sensor did not allow measurements at 45 kVp, which was too close to the operating limits of the device (above 40 kVp). To keep calibration factors at a beam quality sufficiently close to our micro-CT's beam quality in terms of both the tube potential and HVL, the chamber's correction factors at beam quality RQR2 (40 kVp), RQR3 (50 kVp), and RQR4 (60 kVp) were, respectively, applied to the 45, 55, and 65 kVp beams of the nanoSPECT/CT plus^{TM} camera.

CTDI measurements were performed both in a 60 mm diameter PMMA phantom and in a 30 mm diameter PMMA phantom (Table III). In the rat-like phantom, CTDI was found to be equal to 78.0 ± 2.1, 96.7 ± 2.6, and 110.7 ± 3.0 mGy for the nominal settings of the respective protocols M1, M2, and M3. These results were higher by a factor of 1.05, 1.18, and 1.35 compared with the CTDI calculated and displayed by the manufacturer at, respectively, 45, 55, and 65 kVp. In the mouse-like phantom, measured CTDI were 169.3 ± 4.6, 189.8 ± 5.1, and 203.6 ± 5.5 mGy for the commonly used protocols M1, M2, and M3 in whole-body mouse imaging. Accordingly, the radiation dose delivered to mice was much higher than the displayed dose predicted by the manufacturer due to the larger phantom's size used in the computation. Displayed CTDI were underestimated by a factor ranging from 2.29 to 2.48 depending on the voltage settings.

3.B. Nanodots' reproducibility in micro-CT imaging

Table IV shows the reproducibility obtained after ten repeated measurements of ten OSLDs irradiated in phantom B according to each protocol M1, M2, and M3. For each measurement, six OSLDs were placed in the scan range (position from 3 to 8) whereas four OSLDs were outside this range, located on each side (position 1, 2, 9, and 10). Overall CoV of the 30 OSLDs over the ten repeated measurements was better than 2.4% for OSLDs positioned in the scan range and 5.6% for those OSLDs outside the scan range. More precisely, the six central nanoDots exhibited a CoV less than 2.4%, 1.9%, and 2.0% for respective protocols M1, M2, and M3. OSLDs located outside the scan range showed individual variations up to 3.3%, 5.0%, and 5.6% at, respectively, 45, 55, and 65 kVp. The results did not show any change in OSLD sensitivity as a result of the optical treatment.[35] Stability of the x-ray output was checked with the pencil ionization chamber in phantom A. Small variations of less than 0.4% were identified at each of the nominal voltages.

TABLE IV. Reproducibility of OSLD response as a function of nanoDot's position in a mouse-like phantom during micro-CT scans. Experiment was repeated ten times for each protocol (M1, M2, and M3).

	Coefficient of variation (%) for OSLD position no.									
Protocols	1	2	3	4	5	6	7	8	9	10
M1 (45 kVp)	2.6	1.9	1.9	2.1	1.6	1.7	2.4	1.5	2.3	3.3
M2 (55 kVp)	3.0	3.1	1.6	1.4	1.9	1.8	1.0	1.6	2.2	5.0
M3 (65 kVp)	2.0	1.4	2.0	1.8	0.7	1.4	1.6	1.4	2.3	5.6

3.C. Linearity measurements and energy correction

As shown in Fig. 3, OSLD response exhibited a good linearity in the dose range of the micro-CT component of the Bioscan camera, i.e., between 60 and 450 mGy. First point obtained at 45 kVp with protocol L1 was excluded from analysis due to its systematic assignment to the "low-dose" mode during the readout process. Linear regression analysis gave R^2 values of 0.9976, 0.9967, and 0.9969 for respective voltage settings of 45, 55, and 65 kVp. The standard deviations of residuals for these fits were, respectively, 0.4%, 1.2%, and 0.8%. The fit lines showed an intercept of −5.6 ± 2.1, −3.7 ± 2.3, and −4.8 ± 2.2 when extended to zero dose. According to these results, for each voltage, one single energy calibration factor could be used throughout the range of doses delivered by the micro-CT. This calibration factor was used to convert nanoDot's doses to air kerma measured with a properly calibrated CT ionization chamber at low voltages. Given the combined standard uncertainties determined in Sec. 2.G, The slopes of the fit lines were 0.551 ± 0.070, 0.539 ± 0.047, 0.555 ± 0.050 leading to respective energy scaling factors of 1.81 ± 0.23, 1.86 ± 0.16, and 1.80 ± 0.16 at 45, 55, and 65 kVp. Effective photon energy was determined by HVL method.[30] As seen in Sec. 3.A, HVL measurements were 1.63 ± 0.46 mm Al at 55 kVp and 1.89 ± 0.49 mm Al at 65 kVp. Corresponding effective energies were 26.5 ± 5.5 keV at 55 kVp and 28.0 ± 5.5 keV at 65 kVp. Considering the small variations of the ratio of mass energy-absorption coefficients for tissue to air between 15 and 35 keV (<0.6%),[31] a

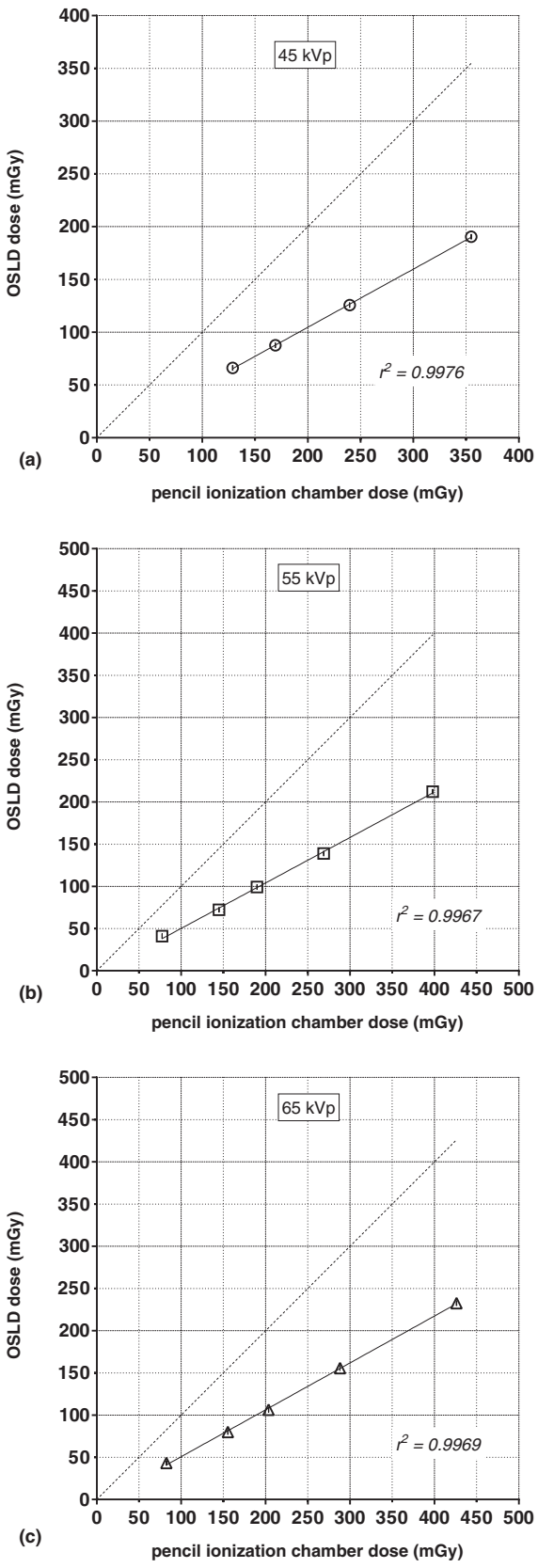

FIG. 3. OSLD dose vs pencil ionization chamber dose for nominal tube voltages of 45 kVp (a), 55 kVp (b), and 65 kVp (c). Solid lines represent regression analysis through the dose points obtained at each voltage. Error bars indicate 1 SD from three repeated measurements with the same OSLD being exposed, read, and then optically annealed. The line of identity is shown as dashed lines for comparison.

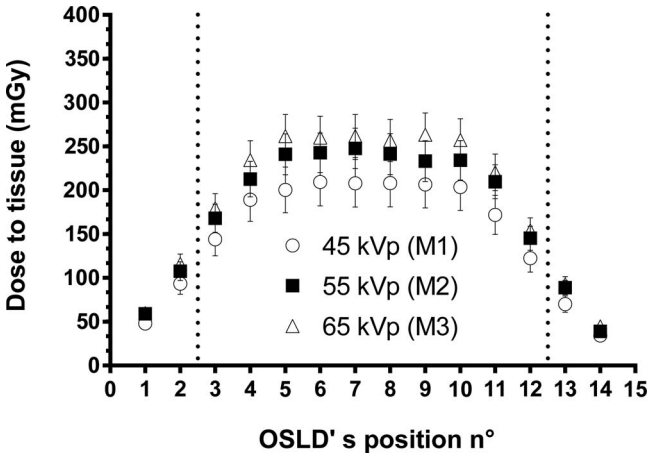

FIG. 4. Axial dose profile obtained at each voltage by exposing 14 OSLDs located in the phantom B and centered over a spiral micro-CT acquisition. Vertical dotted lines represent axial limits of the 10 cm long scan range. Error bars indicate 1 SD from combined standard uncertainties determined in Sec. 2.G.

single factor of 1.05 was subsequently used to convert radiation doses in air to radiation doses in tissue for the three used voltage settings.

3.D. Tissue absorbed doses in phantom and mice

Figure 4 shows the axial dose profile measured with OSLDs inserted in the 30 mm diameter phantom B after a 10 cm long helical CT acquisition. The ten OSLDs located every centimeter at positions 3–12 were in the scan range of the micro-CT. Following energy correction, mean doses to tissue in whole-body CT examination were 186.4 ± 7.6, 217.6 ± 6.6, and 234.9 ± 7.1 mGy at respective voltage 45, 55, and 65 kVp. The dose profile shows that a maximum value was reached after approximately 2 cm in the case of a whole-body spiral CT examination acquired over 10 cm (pitch = 1). Mean doses to tissue over the six most exposed OSLDs (which correspond to the plateau of the dose profile) were 206.0 ± 10.7 240.0 ± 9.4, and 260.2 ± 10.0 mGy for respective protocols M1, M2, and M3.

Table V provides organ doses measured with nanoDots implanted in cadavers following standard whole-body mouse imaging studies acquired with the Bioscan camera of our laboratory. Protocols M1, M2, and M3 correspond to combined irradiations of one topogram (protocol M0) and one micro-CT acquisition with nominal voltage of 45, 55, or 65 kVp. Mean doses to tissue in the mouse trunk (thorax, abdomen, pelvis, and flanks) were 213.0 ± 17.0, 242.6 ± 15.2, and 251.2 ± 13.4 mGy for respective protocols M1, M2, and M3. Extracting the thoracic and abdominopelvic regions (three OSLDs) led to mean doses of 185.7 ± 15.4, 216.0 ± 15.6, and 231.1 ± 17.2 mGy inside the mouse trunk whereas the flanks (two OSLDs) received 253.9 ± 28.2, 282.4 ± 22.5, and 281.3 ± 21.5 mGy at 45, 55, and 65 kVp. OSLDs inserted in the bone cavity of the brain gave mean doses to tissue of 253.4 ± 52.8, 204.6 ± 26.2, and 185.3 ± 20.3 mGy. When positioned outside the mouse (three OSLDs), surface doses were

TABLE V. Organ doses obtained for typical whole-body mouse CT acquisitions with a nanoSPECT/CT plus™ camera. Protocol M0 represents a topogram acquisition. Doses for protocols M1, M2, and M3 arise from topogram M0 plus helical CT acquisitions at respective voltage 45, 55, and 65 kVp. Mean doses are reported with combined standard uncertainties as determined in Sec. 2.G. Mouse trunk represents the mean dose of OSLDs located in the thorax, abdomen, pelvis, and flanks.

	Dose (mGy) for protocols no.				
Organs	M0	M1	M2	M2b	M3
Brain	3.2 ± 0.4	253.4 ± 52.8	204.6 ± 26.2	164.3 ± 16.6	185.3 ± 20.3
Thorax	3.5 ± 0.4	194.4 ± 26.7	224.9 ± 22.4	176.0 ± 16.7	253.5 ± 24.4
Abdomen	3.5 ± 0.5	191.0 ± 26.3	230.8 ± 35.7	150.3 ± 15.5	225.2 ± 23.1
Pelvis	3.0 ± 0.3	171.5 ± 26.8	192.4 ± 20.3	138.5 ± 13.8	214.5 ± 21.5
Right flank	2.0 ± 0.2	276.4 ± 40.9	307.3 ± 37.7	225.5 ± 32.5	284.4 ± 29.5
Left flank	8.5 ± 0.8	231.4 ± 38.9	257.6 ± 24.6	169.8 ± 21.4	278.1 ± 31.4
Head (external)	4.3 ± 0.7	422.0 ± 53.0	311.0 ± 34.1	241.4 ± 28.3	323.9 ± 41.3
Back (external)	6.5 ± 1.4	423.1 ± 64.1	417.3 ± 39.6	289.2 ± 38.1	365.3 ± 36.3
Legs (external)	5.1 ± 0.8	452.4 ± 59.7	460.6 ± 50.1	379.8 ± 38.1	362.5 ± 52.4
Mouse trunk	4.1 ± 0.3	213.0 ± 17.0	242.6 ± 15.2	172.0 ± 11.0	251.2 ± 13.4

much higher with average values of 432.5 ± 34.1, 396.3 ± 24.1, and 350.6 ± 25.3 mGy for respective protocols M1, M2, and M3.

The contribution due to the topogram alone was always less than 2.5% of the total irradiation dose. A noticeable exception was for the OSLD located in the left flank which received a dose of 8.5 mGy during the topogram. This relatively high dose was related to its orientation (front side) and position (before the mouse) with respect to the side orientation of the x-ray tube during the topogram. The use of the multimouse bed of the system allowed for significantly lower doses per animal at each OSLD location (t test, $p < 0.05$). The amount of dose reduction was between 19.7% and 34.1% for internal locations of OSLDs and between 17.5% and 30.7% for OSLDs located externally.

4. DISCUSSION

In this study, the ionization chamber was calibrated in reference to standard radiation qualities corresponding to voltages of 40, 50, and 60 kVp (Table II). HVL was directly measured by positioning a kV-sensor in the primary x-ray field because the conventional experimental set up for HVL measurements could not be performed in the closed gantry of the nanoSPECT/CT plus™ camera.[36] Even though uncertainties associated with direct HVL measurements were rather large (Sec. 2.A), the radiation qualities of the Bioscan's camera were believed to be only slightly different from those required for the ionization chamber and the application of a specific calibration coefficient at each kVp was thought to properly cover the radiation qualities of the micro-CT. Hupfer *et al.* investigated the relative response of a standard pencil ionization chamber in the range of voltages used in micro-CT (40–60 kVp), with one calibration point at 50 kVp.[26] They showed that the deviations (±4%) were in the same order of magnitude as for clinical CT (±6%), with clinical voltages spanning between 100 and 150 kV.

The dosimetric information displayed at the operator console was verified. Using rat-like phantoms, Table III shows that the measured CTDI was found to be between 5.4% and 35% higher than the manufacturer's calculated CTDI. When mouse-like phantoms were used, the displayed CTDI was even less useful in predicting the dose to the animals, underestimating the dose by as much as a factor of 2.48. These results were in accordance with those of Kersemans *et al.* who estimated the absorbed dose of the CT component of the Bioscan camera in a 25.4-mm-diameter phantom using EBT2 gafchromic film (ISP technologies Inc.).[15] By calculating the average dose delivered to the phantom per CT scan, Kersemans *et al.* found that the displayed CTDI was underestimated by a factor of 1.6–2.3 depending on the standard settings used. In order to get a better estimate of absorbed doses in rodents, CTDI values measured in Table III can be used to assess average doses during micro-CT scans of the nanoSPECT/CT plus™ camera.

Reproducibility was investigated in a mouse-like phantom to check the stability of OSLDs sensitivity in the configuration of our CT experiments. For each standard voltage setting, six OSLDs were located in the scan range and the experiment was repeated ten times. The resultant reproducibility of these 18 OSLDs was between 1.9% and 2.4% (1 SD). When partially irradiated on the profile tails of the 6-cm long CT scan, nanoDots showed reproducibility worsened up to 5.6% because the dose delivered was nonuniform over 360° and so was highly dependent on the precise repositioning of OSLDs between repetitive experiments. These results were quite similar to values reported so far in the literature. Al-Senan *et al.* found reproducibility values between 2.9% and 3.6% in the diagnostic range, with a general radiography unit operating at 120 kVp and 80 mAs.[18] At radiation therapy energies, Viamonte *et al.* found reproducibility of an individual detector to be 2.5% after ten repeated irradiations at 50 cGy using ^{60}Co irradiations.[20] Jursinic reported a reproducibility better than 1% for one OSLD repeatedly exposed to 100 cGy with 6 MV x rays.[16] As the number of OSLDs was limited, the

manufacturer's quoted 3% (1 SD) individual sensitivity should be sufficient to account for the batch homogeneity in the general framework of this study. Al-Senan *et al.* reported batch homogeneity between 4% and 5% in the diagnostic range, with observed beam variations of 2%.[18] Reproducibility of exposure was here found to be very stable during helical micro-CT scans (<0.4%).

Linearity of OSLD response with respect to dose was excellent from 60 to 450 mGy. This is in good agreement with published results at diagnostic energies,[18] with supralinearity occurring at doses above 2000–3000 mGy.[16–21] However, this situation needed to be properly investigated because the MicroStar™ reader uses two calibration curves to convert PMT counts to dose. Regarding linearity measurements in Fig. 3, the first point obtained at 45 kVp with protocol L1 was systematically affected to the "low-dose" calibration curve during the readout process and so was discarded from further analysis. Regarding dose measurements in Fig. 4 and Table V, OSLDs exposed to the primary x-ray beam were always processed in the "high-dose" mode except those OSLDs irradiated during a topogram acquired alone (M0). Due to the small contribution of topogram's doses to the helical CT absorbed doses, these were not investigated further.

The Al_2O_3:C OSLDs exhibit a dose response that depends on energy. In the kilo-voltage energies, Al_2O_3:C OSLDs are well known to over-respond due to the increased photoelectric effect that occurs in aluminum oxide ($Z = 11.2$) compared to water ($Z = 7.4$).[21] Also, there is now a growing evidence that ionization density effects that occurred at low energy x rays in small-sized OSLDs could influence OSL properties and so affect the energy response of Al_2O_3:C OSL detectors.[37] In this study, the relative impact of these effects between the radiation qualities of the micro-CT RX beams and the calibrated RX beam (RQR6) was assumed to be negligible and so was not accounted for. Concerning the dose response as a function of energy, OSLDs were provided with a special set of dosimeters to calibrate the MicroStar™ reader in the diagnostic range (80 kVp and a HVL of 2.9 mm Al). In this study, extra energy scaling factors were computed to take into account the lower energy-range used in micro-CT imaging. These factors were found to be 1.81 ± 0.23, 1.86 ± 0.16, and 1.80 ± 0.16 at the respective 45, 55, and 65 kVp voltage settings of the Bioscan camera. Effective energies were assessed to be 26.5 ± 5.5 keV at 55 kVp and 28.0 ± 5.5 keV at 65 kVp. In this range, the manufacturer also proposes precalculated factors to correct for the energy dependence.[29] These factors varies from 1.49 at 16 keV to 1.00 at 44 keV, based on the concept of average energy. In the low-energy diagnostic range, Senan *et al.* calculated factors to be between 0.81 at 29 keV and 1.08 at 40 keV, based on the concept of effective energy.[18] Our own results disagree with the values given by each of these authors. Differences might arise from experimental conditions and dosimetric quantities used. Landaueur provides sets of OSLDs calibrated in terms of primary quantities (air kerma) or operational quantities [Hp(0.07), Hp(10)]. In our study, the computed factors were applied to the air kerma calibrated OSLDs at the RQR6 RX beam quality. They were derived in the presence of scattering media in the exact geometry of our micro-CT imaging studies. We believe that specific user calibrations must be performed in the diagnostic range to avoid misleading use of precalculated energy compensation factors.

Taking into account these preliminary experiments, mean doses to tissue in phantom B were between 186.4 ± 7.6 and 234.9 ± 7.1 mGy during a 10 cm long whole-body CT examination. Axial dose profiles obtained during helical micro-CT acquisitions show that wasted radiation is delivered to the rodents beyond the reconstruction region. As an option, the manufacturer also proposes to flatten the dose profile inside the scan region by overscanning even more to maintain the noise level at both ends of the CT scan. In micro-SPECT/CT imaging, this will result in more and more wasted radiation for a rather small improvement in image quality (see below). Small animal experiments led to similar results with mean absorbed dose to tissue in the mouse trunk found to be between 213.0 ± 17.0 and 251.2 ± 13.4 mGy. The flanks received the highest doses ranging from 253.9 ± 28.2 to 282.4 ± 22.5 mGy, reflecting the subcutaneous positions of the OLSDs. This result must be kept in mind when studying subcutaneous tumor growth during serial imaging of the same animals with the nanoSPECT/CT plus™ camera. Absorbed doses of OSLDs located inside the mouse were generally higher when increasing voltage. The inverse trend was observed for those OSLDs placed externally, which reflects the more penetrating ability of x-ray beams with higher voltage. Absorbed doses in the brain tended also to decrease with increasing energy as a result of the x-ray beam hardening across the bone skull. When positioned on the multimouse bed, the mean absorbed dose per mouse was significantly lower, indicating that these systems could present more advantages than simply increasing the throughput of imaging. Skin doses were found to be rather high with doses to tissue that could reach 450 mGy. This study shows that presets parameters used in standard micro-CT scan can lead to relatively high absorbed doses to small animals with the CT component of the nanoSPECT/CT plus™.

Carlson *et al.* gave a good review of the radiation absorbed dose during micro-CT imaging among different studies in the early 2000s.[8] Absorbed dose in the range 17–760 mGy were found both experimentally using TLD dosimeters and theoretically using Monte Carlo simulations. However, the use of different micro-CT systems with different micro-CT protocols (kVp, mA, number of projections, image time) made comparisons a rather difficult task. It remains that, due to the sampling requirements in small animal imaging, absorbed dose in micro-CT was almost ten times the organ absorbed dose expected in clinical CT,[38] giving rise to questions about a possible radiation therapy effect.

More recently, Figueroa *et al.* found an average absorbed dose to mouse organs of 76 ± 5 mGy using TLD measurements.[9] The micro-CT system used (MicroCAT II™ CT/SPECT, Siemens Medical Solutions, Knoxville, USA) was operating at 80 kVp and 54 mAs, with a HVL of 2.5 mm Al equivalent. The beam was harder than in the present study. The system was reported to produce satisfactory image statistics with radiation doses three to four times lower than

reported here. Rodt *et al.* found that mouse corpses were receiving an average dose of 194 mGy with the beam quality delivered (80 kVp, 1.8 mm Al filter) by the micro-CT system used (eXplore Locus, GEHC, Cahalfont St Giles, UK).[11] Average absorbed doses measured from phantom experiments were in the range 154–229 mGy depending on micro-CT protocols. Willekens *et al.* measured higher radiation doses (295–507 mGy) with TLDs located at the site of different organs in mice.[10] The micro-CT used was a SkyScan 1178 system (SkyScan, Kontich, Belgium). They worked with a standard scan operating at 50 kVp, 0.615 mA and a total acquisition time of 121 s (74 mAs). Reduction of scan times was found to reduce dose at the expense of an exponential increase in noise. Osborne *et al.* conducted dose measurements in mice with nanoDots on the Inveon CT platform (Siemens Medical Solutions, Knoxville, USA).[12] The system was operated at 80 kVp, 0.5 mA, 360 projections of 250 ms per rotation. They found average doses of 138.0 ± 7.4 mGy in the abdomen and 159.9 ± 7.2 mGy at the neck level under the skin. A low-dose detector configuration could drastically lower down these values to, respectively, 9.7 ± 0.5 and 11.8 ± 0.5 mGy with respect to the noise level. Though the authors do not provide any detailed information about nanoDot's calibration at the radiation quality investigated, the study emphasized the compromise that must be kept in mind between image quality (especially noise) and dose.

Indeed, any improvement in image quality will come at the expense of dose. High resolution images will put greater constraints on dose levels unless higher noise is an acceptable solution.[2,3] Solutions to keep high image quality with as little photons as possible require special hardware requirements on x-ray spectrum, x-ray tube power, or CT detectors sensitivity. Additional techniques rely on an efficient use of image processing methods (filtering or iterative reconstruction) so as to lower the dose while keeping the noise level unchanged. However, dose reduction methods in micro-CT have not yet received the same attention as in clinical CT. At the user level, optimization of imaging protocols is a key component of dose reduction. When CT is used only for localization, which is actually the case in SPECT/CT hybrid imaging with the nanoSPECT/CT plus^{TM} camera, optimal choice of kVp, number of projections, and time per projection (mAs per rotation) may have a substantial effect on dose. Though characterizing image quality was not the aim of the present work, no qualitative difference could be observed on the reconstructed images among the three main average protocols M1, M2, and M3 (Fig. 5). Going further, stating that a low-dose micro-CT would be sufficient for localization purposes in hybrid imaging, a dose reduction of 2.6 could be expected in the results shown in Table V by setting adjustable CT parameters to their minimal values (protocol L1 of Table I).

In preclinical studies, serial imaging of the same animals over several time points may be of particular interest in a wide range of applications.[39] For instance, longitudinal studies can be used to study pharmacokinetics of new radiolabeling agents or effectiveness of therapies in suitable animal models. If a global consensus exists to say that radiation

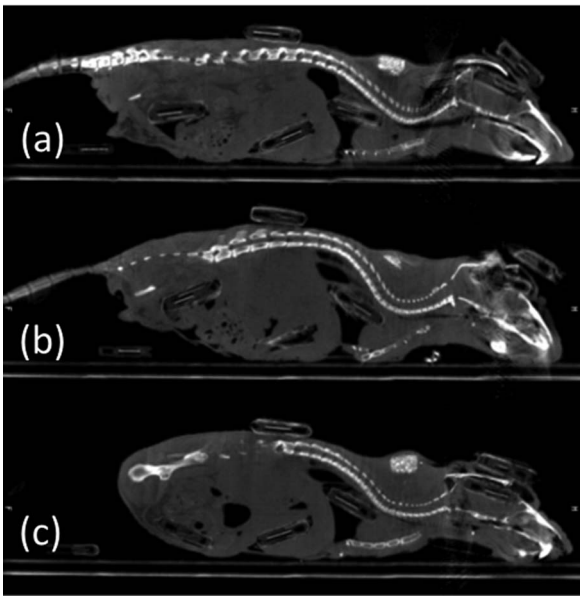

FIG. 5. Sagittal slices of three different mice acquired at, respectively, 45 kVp (a), 55 kVp (b), and 65 kVp (c) with the micro-CT component of the nanoSPECT/CT plus^{TM} camera. The same reconstruction parameters were used.

levels in micro-CT are far from causing deterministic effects,[8] the accumulation of sublethal radiation doses over time could presumably induce biological changes.[10,15] In oncologic studies, it was therefore questioned if the relatively high radiation dose delivered by repetitive micro-CT scans were likely to cause some perturbations to the experimental outcomes. However, this question remains a matter of debate as available results are still rather discordant. Laforest *et al.* observed tumor growth inhibition in mice.[13] The fractionated doses during micro-CT scans were between 60 and 550 mGy, delivered daily or every three days. Foster *et al.* investigated the impact of longitudinal micro-CT imaging on tumor growth in mice and found no radiation dose effects.[14] The rodents were imaged on days 4, 8, 12, and 16 with three different imaging protocols. Even at scanning parameters corresponding to an approximate entrance dose of 300 mGy, no statistically significant differences could be observed in final tumor volumes. Kersemans *et al.* studied biological markers after irradiating mice with the micro-CT component of the nanoSPECT/CT^{TM} camera.[15] They showed that substantial DNA damage could be caused by a single CT scan using standard imaging protocols (65 kVp, 123 μA, 1600 ms, 360 projections). However, these radiation-induced effects were not translated into macroscopic changes. The authors emphasized the need for optimization of scanning parameters, especially in longitudinal studies so as to minimize the biological consequences associated with each scan. The following CT parameters were found to reduce biological effects: 45 kVp, 177 μA, 1600 ms, 180 projections. According to our results, by setting the time per projection to 1500 ms (closest value available on our camera), these parameters would have led to an expected CT chamber dose of 183 mSv (Fig. 3), which is in reasonable agreement with the 150 mSv quoted by the authors, based

on radiographic film analysis. Still, additional optimization is possible in the user mode through the use of a lower time per projection (Table I). Biological responses to low radiation doses are known to be quite complex and nonfully understood at present. More studies are needed to assess the biological impact of serial micro-CT scans and investigate the full spectrum of low-dose effects which might be induced in small animals.

As in the clinical environment, the preclinical systems are now often available as integrated hybrid cameras. In radioisotope imaging coupled to CT, the radiopharmaceutical dose will add to the total dose delivered to the animals. In SPECT and PET imaging, Funk *et al.* estimated the total whole-body dose of small animals to be between 60 and 900 mGy, depending on isotope and administered activity.[40] The optimization effort must be conducted in both modalities to ensure that the highest image quality is obtained with the smallest dose delivered to rodents. Preclinical scientists are not always aware of this compromise, especially as the desired image quality is not necessarily known *a priori*.

In comparison with TLD detectors, OSLDs were relatively easy to handle and to process using the MicroStar™ reader. Regarding dose measurements in the diagnostic range, three main sources of errors have already been identified with OSLDs: adding small doses to an OSLD which has already high accumulated doses (which is not the case in the present study), angular and energy dependence.[18] Angular dependence was shown to be minimal in CT where measurements were averaged over numerous projections acquired during a 360° rotation. Therefore, a 10% maximum variability in dose measurements was measured in clinical CT.[18] In this study, topograms were acquired with OSLDs facing the x-ray beam. In micro-CT scans, OSLDs were always aligned along the bed axis in phantoms and as close as possible to this alignment in cadavers so that the angular dependence was believed to be minimal. Energy dependence was taken into account accordingly. The main drawbacks of OSLDs in the present study came from the nanoDots' dimensions which were rather large compared to the mouse size. Also, statistics could have been improved in two ways: first, screened dosimeters could have been used which could theoretically lead to better homogeneity of a given batch (1% at 1 SD). Second, relative sensitivity factors could have been determined individually through specific calibration at relevant energies. As a whole, OSL dosimetry has proven here to be an attractive alternative to TLD measurements in small animal imaging.

5. CONCLUSIONS

OSLDs can be used effectively as a surrogate to TLDs for dose measurements in small animal experiments. With proper energy correction, radiation dose can be assessed quickly and easily with a reasonable precision in the low-kV range (±10%). Using this technique, average doses delivered to mice using the standard settings of the micro-CT component of the nanoSPECT/CT plus camera™ were found to be relatively high for the only purpose of localization, while the need of high quality images is not necessarily justified. In order to minimize potential radiation-induced adverse effects of micro-CT serial imaging on experimental outcomes, acquisition parameters in hybrid SPECT/CT imaging have to be optimized to draw the best dose reduction capabilities of the microsystem used.

ACKNOWLEDGMENTS

This work was realized in collaboration with Bioscan Inc. in the framework of a traineeship agreement. The authors would like to thank J. Burnet, Y. Chevalier, S. Pesnel, and H. Haas from Bioscan Inc. for helpful discussions on technical information regarding the micro-CT unit of the nanoSPECT/CT plus™ camera. This work has benefited of a French government grant managed by the French National Research Agency (ANR) under the program "Investissements d'avenir" with reference ANR-10-EQPX-05-01.

[a]Author to whom correspondence should be addressed. Electronic mail: jmvrigneaud@cgfl.fr; Telephone: +33 3 45 34 80 55; Fax: +33 3 80 73 77 32.

[1]M. J. Paulus, S. S. Gleason, S. J. Kennel, P. R. Hunsicker, and D. K. Johnson, "High resolution X-ray computed tomography: An emerging tool for small animal cancer research," Neoplasia **2**(1–2), 62–70 (2000).
[2]S. H. Bartling, W. Stiller, W. Semmler, and F. Kiessling, "Small animal computed tomography imaging," Curr. Med. Imaging Rev. **3**(1), 45–59 (2007).
[3]N. L. Ford, M. M. Thornton, and D. W. Holdsworth, "Fundamental image quality limits for microcomputed tomography in small animals," Med. Phys. **30**(11), 2869–2877 (2003).
[4]R. A. de Kemp, F. H. Epstein, C. Catana, B. M. W. Tsui, and E. L. Ritman, "Small-animal molecular imaging methods," J. Nucl. Med. **51**(Suppl. 1), 18S–32S (2010).
[5]J. M. Boone, O. Velazquez, and S. R. Cherry, "Small-animal X-ray dose from micro-CT," Mol. Imaging **3**(3), 149–158 (2004).
[6]R. Taschereau, P. L. Chow, and A. F. Chatziioannou, "Monte Carlo simulations of dose from microCT imaging procedures in a realistic mouse phantom," Med. Phys. **33**(1), 216–224 (2006).
[7]P. Deak and W. A. Kalender, "A Monte Carlo tool for micro-CT dose assessment," in *World Congress on Medical Physics and Biomedical Engineering, Munich, Germany, 7–12 September 2009*, edited by O. Dössel and W. C. Schlegel (Springer, Berlin, 2009), pp. 338–341.
[8]S. K. Carlson, K. L. Classic, C. E. Bender, and S. J. Russell, "Small animal absorbed radiation dose from serial micro-computed tomography imaging," Mol. Imaging Biol. **9**(2), 78–82 (2007).
[9]S. D. Figueroa, C. T. Winkelmann, H. W. Miller, W. A. Volkert, and T. J. Hoffman, "TLD assessment of mouse dosimetry during microCT imaging," Med. Phys. **35**(9), 3866–3874 (2008).
[10]I. Willekens *et al.*, "Evaluation of the radiation dose in micro-CT with optimization of the scan protocol," Contrast Media Mol. Imaging **5**(4), 201–207 (2010).
[11]T. Rodt *et al.*, "Phantom and cadaver measurements of dose and dose distribution in micro-CT of the chest in mice," Acta Radiol. **52**(1), 75–80 (2011).
[12]D. R. Osborne, S. Yan, A. Stuckey, L. Pryer, T. Richey, and J. S. Wall, "Characterization of X-ray dose in murine animals using microCT, a new low-dose detector and nanoDot dosimeters," PLoS ONE **7**(11), e49936 (2012).
[13]R. Laforest, C. E. Waterson, S. M. Broski and J. S. Lewis, "Radiation dose considerations in tumor growth monitoring with CT," Mol. Imaging **3**(3), 288 (2004).
[14]W. K. Foster and N. L. Ford, "Investigating the effect of longitudinal micro-CT imaging on tumour growth in mice," Phys. Med. Biol. **56**(2), 315–326 (2011).
[15]V. Kersemans *et al.*, "Micro-CT for anatomic referencing in PET and SPECT: radiation dose, biologic damage, and image quality," J. Nucl. Med. **52**(11), 1827–1833 (2011).

[16]P. A. Jursinic, "Characterization of optically stimulated luminescent dosimeters, OSLDs, for clinical dosimetric measurements," Med. Phys. **34**(12), 4594–4604 (2007).
[17]E. G. Yukihara and S. W. S. McKeever, "Optically stimulated luminescence (OSL) dosimetry in medicine," Phys. Med. Biol. **53**(20), R351–R379 (2008).
[18]R. M. Al-Senan and M. R. Hatab, "Characteristics of an OSLD in the diagnostic energy range," Med. Phys. **38**(7), 4396–4405 (2011).
[19]V. Schembri and B. J. M. Heijmen, "Optically stimulated luminescence (OSL) of carbon-doped aluminum oxide (Al_2O_3:C) for film dosimetry in radiotherapy," Med. Phys. **34**(6), 2113–2118 (2007).
[20]A. Viamonte, L. A. R. da Rosa, L. A. Buckley, A. Cherpak, and J. E. Cygler, "Radiotherapy dosimetry using a commercial OSL system," Med. Phys. **35**(4), 1261–1266 (2008).
[21]C. S. Reft, "The energy dependence and dose response of a commercial optically stimulated luminescent detector for kilovoltage photon, megavoltage photon, and electron, proton, and carbon beams," Med. Phys. **36**(5), 1690–1699 (2009).
[22]P. A. Jursinic, "Changes in optically stimulated luminescent dosimeter (OSLD) dosimetric characteristics with accumulated dose," Med. Phys. **37**(1), 132–140 (2010).
[23]J. R. Kerns, S. F. Kry, N. Sahoo, D. S. Followill, and G. S. Ibbott, "Angular dependence of the nanoDot OSL dosimeter," Med. Phys. **38**(7), 3955–3962 (2011).
[24]M. A. Keenan, M. G. Stabin, W. P. Segars, and M. J. Fernald, "RADAR realistic animal model series for dose assessment," J. Nucl. Med. **51**(3), 471–476 (2010).
[25]National Electrical Manufacturers Association, NEMA Standard Publication NU 4-2008: *Performance Measurements of Small Animal Positron Emission Tomo-Graphs* (National Electrical Manufacturers Association, Rosslyn, VA, 2008).
[26]M. Hupfer, D. Kolditz, T. Nowak, F. Eisa, R. Brauweiler, and W. A. Kalender, "Dosimetry concepts for scanner quality assurance and tissue dose assessment in micro-CT," Med. Phys. **39**(2), 658–670 (2012).
[27]International Electrotechnical Commission (IEC) Publication 61267, *Medical diagnostic x-ray equipment-Radiation conditions for use in the determination of characteristics*, 2nd ed. (2005).
[28]D. Gutierrez and H. Zaidi, "Assessment of scatter for the micro-CT subsystem of the trimodality FLEX Triumph preclinical scanner," Med. Phys. **38**(7), 4154–4165 (2011).
[29]C. J. Yahnke, R. D. Hanify and M. R. Salasky, *MicroStar Calibration Conversion Factors for Dots* (Landauer Inc., Glenwood, IL, USA, 2008).
[30]D. J. Dowsett, P. A. Kenny, and R. E. Johnston, *The Physics of Diagnostic Imaging*, 2nd revised ed. (CRC Press, London, GB, 2006).
[31]J. M. Boone and A. E. Chavez, "Comparison of x-ray cross sections for diagnostic and therapeutic medical physics," Med. Phys. **23**(12), 1997–2005 (1996).
[32]P. Workman *et al.*, "Guidelines for the welfare and use of animals in cancer research," Br. J. Cancer **102**(11), 1555–1577 (2010).
[33]International Atomic Energy Agency, *Measurement Uncertainty: A Practical Guide for Secondary Standards Dosimetry Laboratories* (International Atomic Energy Agency, Vienna, 2008).
[34]P. R. Bevington and D. K. Robinson, *Data Reduction and Error Analysis for the Physical Sciences*, 3rd revised ed. (McGraw Hill Higher Education, New York, 2002).
[35]A. A. Omotayo, J. E. Cygler, and G. O. Sawakuchi, "The effect of different bleaching wavelengths on the sensitivity of Al(2)O(3):C optically stimulated luminescence detectors (OSLDs) exposed to 6 MV photon beams," Med. Phys. **39**(9), 5457–5468 (2012).
[36]R. L. Kruger, C. H. McCollough, and F. E. Zink, "Measurement of half-value layer in x-ray CT: A comparison of two noninvasive techniques," Med. Phys. **27**(8), 1915–1919 (2000).
[37]P. B. R. Gasparian, F. Vanhavere, and E. G. Yukihara, "Evaluating the influence of experimental conditions on the photon energy response of $Al2O_3$:C optically stimulated luminescence detectors," Radiat. Meas. **47**(4), 243–249 (2012).
[38]P. C. Shrimpton, M. C. Hillier, M. A. Lewis, and M. Dunn, "National survey of doses from CT in the UK: 2003," Br. J. Radiol. **79**(948), 968–980 (2006).
[39]G. C. Kagadis, G. Loudos, K. Katsanos, S. G. Langer, and G. C. Nikiforidis, "In vivo small animal imaging: Current status and future prospects," Med. Phys. **37**(12), 6421–6442 (2010).
[40]T. Funk, M. Sun, and B. H. Hasegawa, "Radiation dose estimate in small animal SPECT and PET," Med. Phys. **31**(9), 2680–2686 (2004).